Valentin Demidov*, Vladislav Toronov, Yuan Xu, Barry Vuong, Carry Sun, Victor Yang and Alex Vitkin

Imaging the electro-kinetic response of biological tissues with phase-resolved optical coherence tomography

Darstellung der elektrokinetischen Reaktion von biologischen Geweben mittels phasenaufgelöster optischer Kohärenztomographie

Abstract: In this study, the electro-kinetic phenomena (EKP) induced in biological tissue by external electric field, while not directly visible in optical coherence tomography (OCT) images, were detected by analyzing their textural speckle features. During application of a low-frequency electric field to the tissue, speckle patterns changed their brightness and shape depending on the local tissue EKP. Since intensities of OCT image speckle patterns were analyzed and discussed in our previous publications, this work is mainly focused on OCT signal phase analysis. The algorithm for extracting local spatial phase variations from unwrapped phases is introduced. The detection of electrically induced optical changes manifest in OCT phase images shows promise for monitoring the fixed charge density changes within tissues through their electro-kinetic responses. This approach may help in the identification and characterization of morphology and function of healthy and pathologic tissues.

Keywords: phase; optical coherence tomography; electro-kinetic phenomenon; OCT image processing; optical properties of tissue.

***Corresponding author: Valentin Demidov,** Department of Medical Biophysics, University of Toronto, 101 College Street, Toronto, ON M5G 1L7, Canada, e-mail: val.demidov@mail.utoronto.ca
Vladislav Toronov and Yuan Xu: Department of Physics, Ryerson University, 50 Gould Street, Toronto, ON, M5B 2K3, Canada
Barry Vuong and Victor Yang: Department of Electrical and Computer Engineering, Ryerson University, 50 Gould Street, Toronto, ON, M5B 2K3, Canada
Carry Sun: Department of Medicine, University of Toronto, 610 University Avenue, Toronto, ON, M5G 2M9, Canada; and Department of Electrical and Computer Engineering, Ryerson University, 50 Gould Street, Toronto, ON, M5B 2K3, Canada
Alex Vitkin: Department of Medical Biophysics, University of Toronto, 101 College Street, Toronto, ON M5G 1L7, Canada; and Department of Radiation Oncology, University of Toronto, 610 University Avenue, Toronto, ON, M5G 2M9, Canada

Zusammenfassung: In dieser Studie wurden die elektrokinetischen Phänomene (EKP) in biologischem Gewebe, die durch ein äußeres elektrisches Feld induziert wurden, jedoch nicht direkt mittels optischer Kohärenztomographie (optical coherence tomography, OCT) dargestellt werden können, durch die Analyse ihrer strukturellen Speckle-Merkmale erfasst. Wie sich zeigte ändern die Speckle-Muster während der Anwendung eines niederfrequenten elektrischen Feldes ihre Helligkeit und Form in Abhängigkeit von den lokalen EKP des Gewebes. Während in unseren früheren Veröffentlichungen die Intensitäten der Speckle-Muster in den OCT-Bildern analysiert wurden, fokussiert sich die vorliegende Arbeit auf die Signal-Phasenanalyse und stellt einen entsprechenden Algorithmus zur Extraktion lokaler räumlicher Phasenvariationen vor.

Die Detektion von elektrisch induzierten optischen Veränderungen die sich in den OCT-Phasenbildern manifestieren scheint für das Monitoring fester Ladungsdichteveränderungen im Gewebe durch ihre elektrokinetische Reaktion vielversprechend. Dieser Ansatz kann bei der Identifizierung und Charakterisierung der Morphologie und Funktion von gesunden und pathologischen Geweben helfen.

Schlüsselwörter: Phase; optische Kohärenztomographie; elektrokinetisches Phänomen; OCT-Bildverarbeitung; optische Gewebeeigenschaften.

DOI 10.1515/plm-2014-0027
Received June 17, 2014; revised August 7, 2014; accepted August 11, 2014; previously published online September 12, 2014

1 Introduction

An external electric field applied to biological tissue may trigger various effects, related to the electro-kinetic

phenomena (EKP) [1]. These effects stem from the motion of particles and fluids under the influence of an electric field [2]. EKP depend on many parameters including fixed charge density, electrical conductivity, local environment, hydraulic permeability, ion diffusivity, and stiffness [3]. Applied electric field thus affects cells and biological tissues in various complex ways. Different electric field-induced effects have been investigated using optical microscopy *in vitro* in colloid, blood, and cell culture, to image changes in cellular shape [4], orientation [5] and migration [6].

Recently EKP has been imaged in various intact soft biological tissues *ex vivo* [7–9]. In particular, ultrasound was employed to image the electric field-induced mechanical change (EIMC) in bulk tissues including deformation and strain [8]. It was concluded that the EIMC in soft biological tissues was related to EKP [9]. Similarly, the surface displacements of cartilage tissue due to applied electric field were measured using optical reflectometry [10]. It was shown that the surface displacements increased with voltage and were inversely proportional to the frequency of the applied electric field. The periodic electric fields applied to biological tissue in our previous one-dimensional experiments were seen to influence the optical coherence tomography (OCT) signal amplitude significantly, and in synchrony with the applied fields [11]. The detected signal oscillations were likely caused by the field-shifted tissue interstitial fluids, which may change light scattering and absorbance by affecting the mutual alignment of collagen fibrils [12]. Further investigations [13] revealed that the amplitude of the OCT signal change varied with the magnitude of the applied field and was inversely proportional to its frequency. More recently, Peña et al. [14] used OCT amplitude images to visualize the propagation of low-frequency electric field in tissue samples *ex vivo*, invoking the mechanism of electrically induced optical changes (EIOC) related to the electro-kinetic properties of tissue [14].

In this work, the EKP in soft biological tissues through the phase changes of OCT signal is further investigated. OCT measures the depth-resolved reflectivity of scattering materials by detecting backscattered light [15]. An OCT system interferes with the reflections from a sample with a reference beam originating from the same light source and reflected off a reference mirror. From the resulting interference signal, the sample reflectivity profile along the beam axis can be derived. This one-dimensional depth scan is called the A-scan, in analogy to ultrasound imaging. OCT systems perform many adjacent A-scans in order to create two- (2D) or three-dimensional images of the sample. A-scans can be acquired either in the time domain or in the frequency domain. In this study the frequency domain OCT was used, in particular, swept source OCT (SS-OCT) [16].

A SS-OCT system acquires A-scans with a fixed reference path (non-moving reference mirror) by measuring the spectral response of the interferometer. With a tunable light source, a sweep over a range of optical frequencies is performed. The interference signal is measured at the output with a photo detector. The information is then encoded as an interferogram in the optical frequency space – a sum of oscillations with different frequencies corresponding to reflections from different depths. An inverse Fourier transform then yields the reflectivity as a complex (amplitude and phase) function of depth, i.e. the depth reflectivity profile of the sample.

In the present study, the SS-OCT signal phase changes induced by the electric field in biological tissues as a function of time is demonstrated. New imaging schemes and data analysis methodologies are applied to OCT images of tissue to study EKP, in an effort to enrich the information provided by standard amplitude-based OCT. The algorithm for extracting local spatial phase variations is proposed. The phase images related to the electro-kinetic properties of tissue are derived and compared with corresponding OCT structural phase images.

2 Materials and methods

2.1 Specimen preparation

Tissue samples (~6×3×1.5 cm^3), prepared from the tricuspid valves of fresh porcine hearts, were used as specimens because of their high electrical conductivity [17]. Each sample was clamped into a Plexiglas® frame to reduce mechanical motion as shown in Figure 1. Electrodes made of 24 AWG PVC (7×32) tinned copper wire (Belden Inc., Richmond, IN, USA) were placed 6 cm apart on the opposite sides of the surface of the sample. Each electrode was covered with Spectra® 360 electrically conductive gel (Parker Laboratories, Fairfield, NJ, USA) to improve the electrical contact. A synthesized function generator (model DS335; Stanford Research Systems, Sunnyvale, CA, USA) was used as power source to generate square-wave electrical signals of 10 V magnitude at 0.1 Hz frequency. A thin layer plastic membrane (Resinite packaging film; AEP Canada Inc., Scarborough, Canada) was placed over top of the sample to reduce dehydration. Each specimen was left at room temperature for 5 h before the experiment to ensure thermal equilibrium.

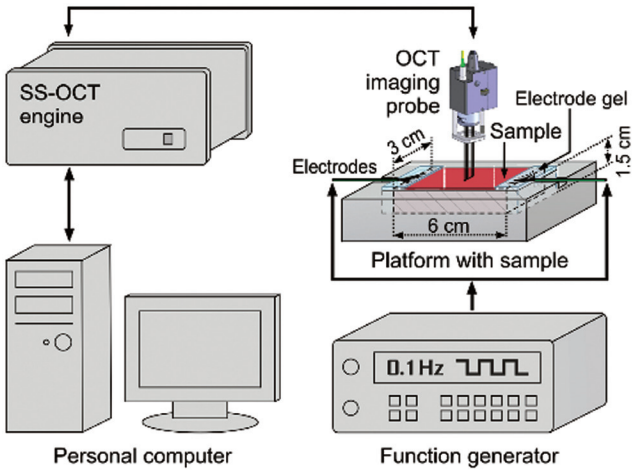

Figure 1 Schematic presentation of the experimental set-up.

2.2 OCT instrumentation

A fiber-based SS-OCT system (model #SL1325-P16; Thorlabs, Newton, NJ, USA) employed a broadband light source with a central wavelength of 1310 nm and spectral bandwidth of 70 nm. The system's optical axial and transverse resolutions were 10.8 μm and 25 μm in air, respectively. The detector signal was digitized using a 16-bit 1.25 MHz data acquisition card (PCIe-6363; National Instruments, Austin, TX, USA) with a sampling speed of 50 MS/s. A SS-OCT microscope software (version 2.3.0; Thorlabs) running on a personal computer (3.6-GHz dual-core processor; Intel) managed data acquisition and image display. The data was collected in the form of interference fringes data points which were processed to form 1024-pixel-wide×512-pixel-deep complex frames that were later used to calculate phase images (real depths for all depth-resolved images in this paper were calculated using an average tissue refractive index n=1.4). Imaging speed was one frame per second to assure adequate sampling. Consistent with the pixilation numbers above, each frame contained 1024 A-scans (3 mm laterally).

2.3 Experimental procedure

Measurements with different cardiac tissue samples were performed to investigate the effects of a low-frequency electric field (0.1 Hz) on the backscattered signal-phase changes in 2-D (B-mode) OCT phase images. A-scans were obtained with the probe scanning laterally along the middle of the sample (3 cm from each electrode) with and without an applied electric field. The longest dimension of the sample was positioned perpendicular to the OCT probe. The B-mode OCT images were organized in frames of 1024 consecutive A-scans (1024×512 pixels images) with axial scan rate of 16 kHz as shown in Figure 2. Images were acquired every second. Each experiment lasted for 480 s with the alternating current (AC) voltage application within the interval from 120 to 300 s.

2.4 Development of phase imaging algorithm

The approach to process the phase of OCT signals involved several steps which are summarized in Figure 3 and briefly discussed below:

- *Step 1: Raw phase extraction.* There exists a variety of methods of phase extraction from interferograms. The phase shifting approach [18] is a popular technique for phase estimation; however, its application is limited by the requirement of multiple frames. For phase estimation using a single frame, several methods have been proposed, including Fourier transform [19], regularized phase tracking [20], high-order ambiguity function [21], windowed Fourier transform [22], dilating Gabor transform [23], Wavelet transform [24], and Wigner-Ville distribution [25]. Here, the classic one, the Fourier transform method, for robustness and ease of use was used. After inverse Fourier transform of each interferogram, a four-quadrant inverse tangent of imaginary-to-real-parts ratio was calculated for resulting complex OCT signal frame pixel-by-pixel for phase estimation.
- *Step 2: Phase unwrapping.* At this step, each A-line of each frame was unwrapped to correct phase angles by adding multiples of $\pm 2\pi$ when absolute jumps between adjacent phase values were greater than or equal to π radians. The typical resulting temporal profile of one A-line (A-scanning in time at the same mirror position) is shown in Figure 4. The periodic changes in optical signal phase between 120 and 300 s of the experiment reflect the periodic change of the polarity of external electric field in the same time interval (36 changes of polarity in 18 full cycles during 3 min of AC application). These oscillations are clearly seen because the field shifts the interstitial fluids periodically, which changes light scattering and absorbance by affecting the mutual alignment of collagen fibrils in tissue [12].
- *Steps 3–4: Extracting local phase features by angular de-trending.* After forming a single axial profile from each frame containing 1024 A-lines, smoothing (step 3) and angular de-trending (step 4) were

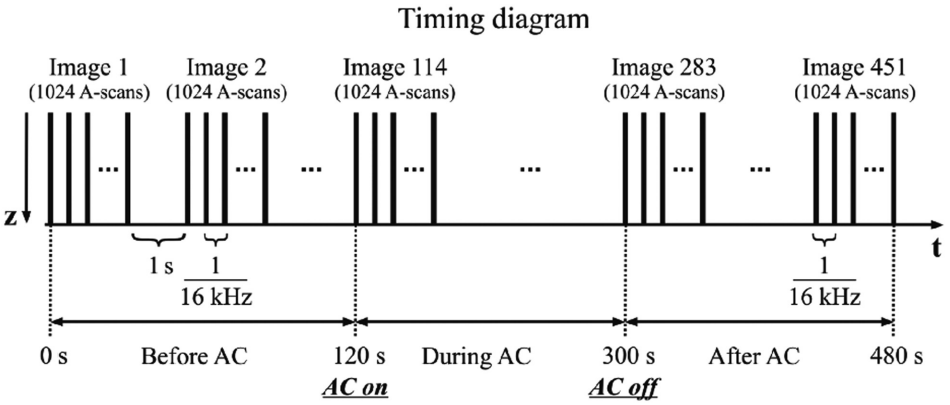

Figure 2 Timing diagram for data acquisition.

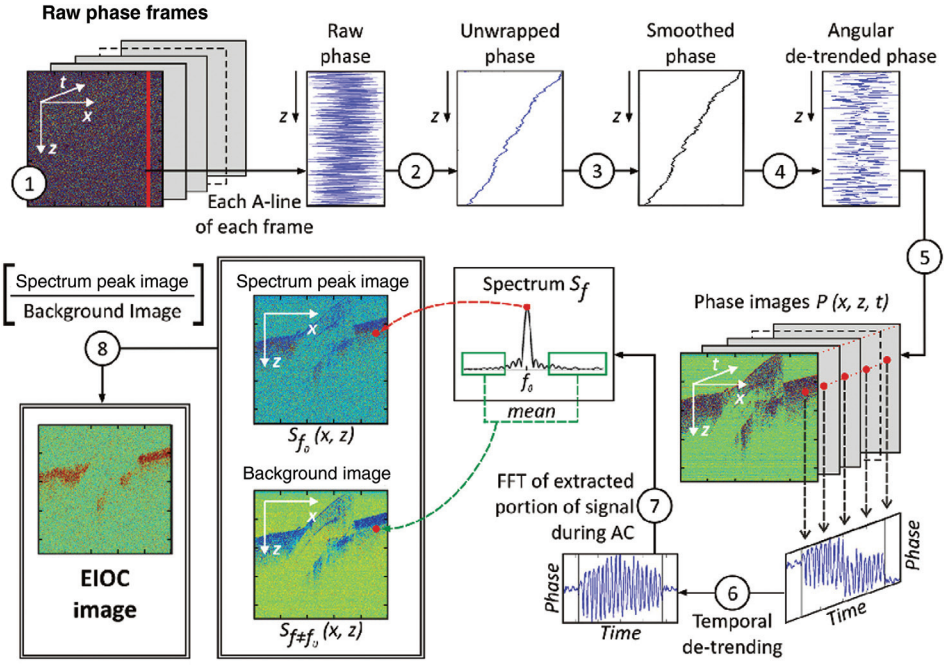

Figure 3 Diagram of the 2-D phase image processing algorithm, showing the analysis path from raw phase image (top left, step 1) to the electrically induced optical changes (EIOC) image (bottom left, step 8). FFT, fast Fourier transform.

applied. As shown in Figure 5, the necessity of these steps rose from the fact that optical phase noise significantly affects the quality of resulting phase signals. Figure 5A illustrates the unwrapped phase before the application of electric field to the sample (t=38 s) for one of the A-scans. Ideally, before electric field application all unwrapped phases should be identical but significant fluctuations about the general trend caused by mechanical movements of the laterally scanning probe and vibrations of the experimental set-up were noted (Figure 5B). In order to eliminate this random fluctuation and obtain the local phase changes, angular de-trending was implemented. Each unwrapped phase curve was smoothed within the range of the nearest five points (Figure 5A inset) and subtracted from the original unwrapped curve to get the local phase features. The five points smoothing range was selected such as not to exceed [-π; π] range of the resulting angular de-trended phase.

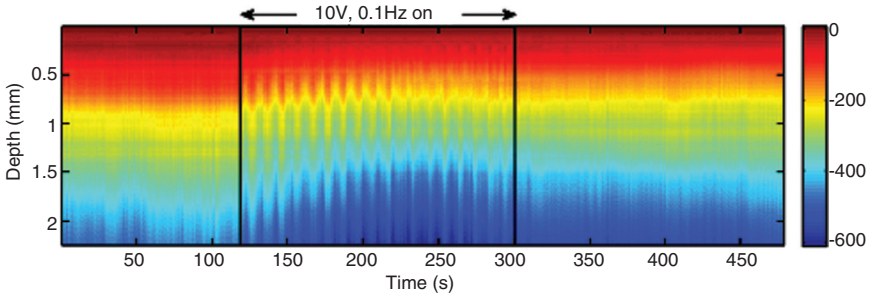

Figure 4 Typical unwrapped phase temporal profile of one A-line, with the scale bar in radians on the right. Eighteen oscillations within 180 s of 0.1-Hz electric field application show the match of the external driving force and internal changes in tissue reflected by changes in backscattered signal phase.

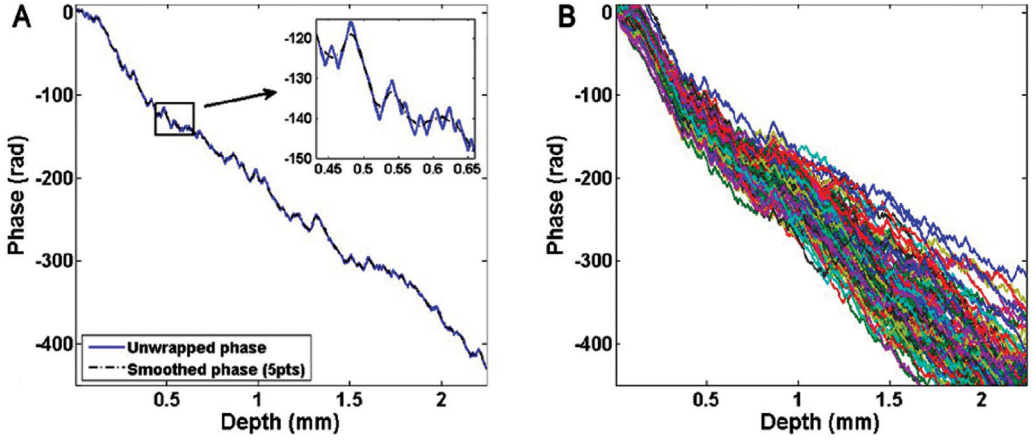

Figure 5 Unwrapped phase curves before application of electric field to the tissue: (A) single A-scan, t=38 s, and (B) all A-scans at the same lateral mirror position, t=1–110 s.

The rest of the signal processing algorithm shown in Figure 3 to obtain the EIOC phase image (steps 5–8) was similar to our previous work on OCT signal amplitude analysis [13]. Briefly, for each pixel's angular de-trended phase in time, the temporal de-trending procedure was applied to eliminate the slow trend in the signal, and thus filter out the spurious frequencies in the spectrum obtained in the following step. The extracted portion of the signal during AC application was Fourier-transformed to calculate the frequency and the magnitude of OCT signal phase change. Two sets of images (not phase images of themselves) were formed: 1) from the peak spectrum magnitude around the frequency of external electric field at f_0=0.1 Hz (spectrum peak image); and 2) from the spectrum magnitudes averaged over all frequencies except a small interval around f_0 and the corresponding harmonics (background image). Finally, the spectrum peak image was divided pixel-by-pixel by the background image to obtain the EIOC phase image.

3 Results

The developed algorithm for extracting phase variations from unwrapped phases was used to obtain phase images of the tissue, representing information about the local phase variation as a function of space. As seen in Figure 6A, raw signal phases calculated from complex OCT signals carry no visually-obvious information. Averaging of many frames simply filters out much of the useful signal phase which becomes close to zero (Figure 6B). However, phase images obtained after angular de-trending procedure (Figure 6C) and carrying the information about the local phase variations, reflect the local structural features of tissue (somewhat analogous to the amplitude image demonstrated in [13]).

A 1-mm diameter dielectric (i.e., electrically insulating) optical fiber, seen in the middle of the sample in Figure 6C, was inserted at an arbitrary angle to represent a negative control in order to verify the ability of the technique

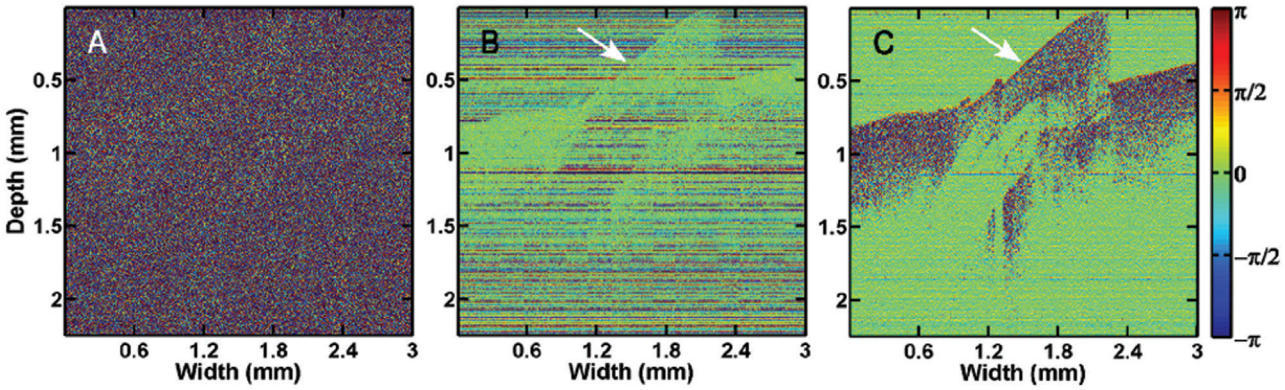

Figure 6 (A) One of the raw phase images (t=88 s), (B) the averaged (110 frames) raw phase image with the useful signal phase being washed out, and (C) angular de-trended phase image. A 1-mm diameter optical fiber, marked with white arrows in (B) and (C), that was inserted in the middle of the sample is present in all three images. Color bar is in radians.

to image the electro-kinetic properties of tissue. In the figure, the optical fiber cladding material surrounding the transparent core can clearly be distinguished. During application of external electric field to the sample, the electrophoresis leads to the liquid flow towards the direction of the field [26] and, therefore, causes changes in the backscattered signal amplitude and phase. If the liquid flow is impeded, there should be minimal changes in the local backscattered signal phase; thus, the insulating optical fiber should be nearly invisible in the resulting EIOC phase image. Further, if there is no electric field presented (thus no EKP in tissue), the resulting EIOC image should carry no information except background fluctuations.

A simple experiment was conducted to demonstrate this. The same algorithm as seen in Figure 3 was applied to get EIOC images before, during and after electric field application to tissue sample. The resulting images are shown in Figure 7. There are nine images divided into three categories. The top row represents the spectrum peak images, the middle row the background images and the bottom row the EIOC images.

As demonstrated in Figure 7A and B for images before AC application and Figure 7G and H for images after AC application, there is no useful information about EKP in the absence of the electric field. Consequently, the corresponding EIOC images (Figure 7C and I) for both cases carry no information. During AC, however, the background fluctuations give rise to non-zero Fourier transform values at f_0, making the optical fiber visible on the spectrum peak image and concealing the electro-kinetic response, although there is obviously no electric current induced inside the dielectric fiber. After removing the background fluctuations (Figure 7E), the fiber and a small region of surface tissue to the left of the fiber in Figure 7D disappeared, in agreement with the absence of electric current in them. Thus it can be concluded that the EIOC image obtained during electric field application (Figure 7F) represents the information related to the tissue electro-kinetic response.

4 Discussion

The feasibility of the five points smoothing range selected for angular de-trending as not to exceed [-π; π] range needs further exploration. Figure 8 demonstrates how different smoothing ranges affect the resulting phase images in B-mode if [-π; π] angular de-trending range is exceeded. Three unwrapped phase curves are shown in the top row of Figure 8, with corresponding phase images at the bottom (Figure 8A–C). With increasing number of points for smoothing of unwrapped phase curve, the noise level increases, causing degradation of the final phase image. For 21 nearest points smoothing (Figure 8B), phase image loses its sharpness; for 45 points (Figure 8C), it becomes so blurred that only contour of the sample can be distinguished.

EIOC images for both amplitude and phase variations of OCT signal during application of external electric field were calculated. As both depend on backscattering properties of tissue, it was expected that corresponding EIOC images would show some similarities and some differences. Indeed, the OCT speckle pattern formation depends on the microscopic structure of the measured object resulting from the interference of backscattered light from the ensemble of scatterers in the tissue. Speckles are known to contain information about scatterers' average properties (distribution, size, and shape) without individually resolving them [27]. Due to the application of the low-frequency external electric field, speckle patterns change their

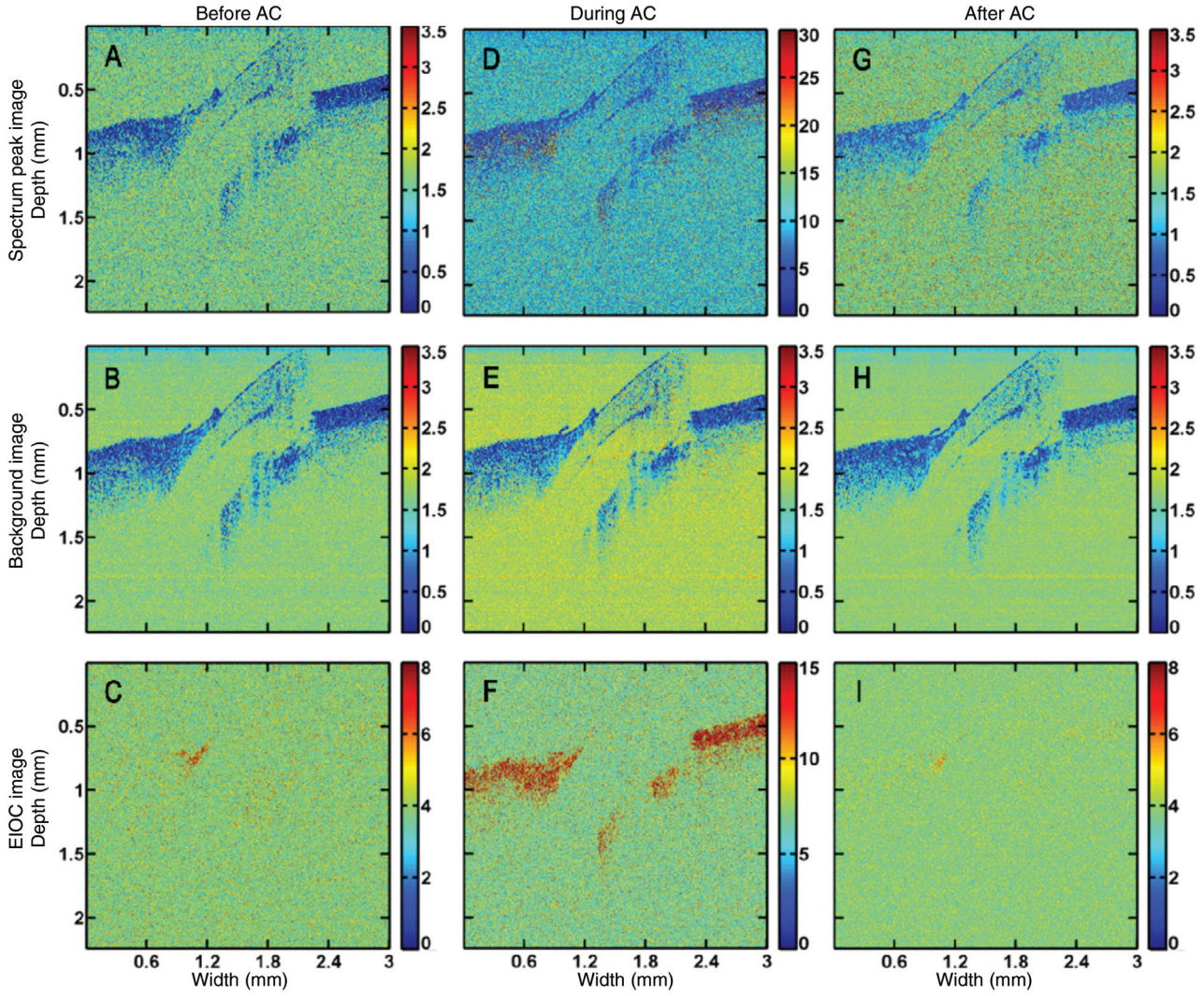

Figure 7 Top row: Peak spectrum images before (A), during (D) and after (G) AC application. Middle row: Background images before (B), during (E) and after (H) AC application. Bottom row: electrically induced optical changes (EIOC) phase images before (C), during (F) and after (I) AC application. Note that before and after AC application the resulting images (C) and (I) carry no information due to absence of electric current in the sample while (F) clearly demonstrates the difference during AC application.

brightness and shape in resulting OCT images depending on the local EKP. The EIOC amplitude image therefore may represent the relative magnitude of electric field influence on tissue through changes of intensity of these speckle patterns. EIOC phase image, in turn may reflect the electric field influence on sub-resolution scatterers distribution. As comparison of Figure 9A and B reveals, the EIOC amplitude and phase images exhibit many common features like tissue boundaries around optical fiber (fiber was seen in the initial spectrum peak image but was filtered out after background removal) and tissue sample surface, but also some differences. To explore these further, Figure 9C demonstrates their 2-D inter-image cross-correlation image $C(i, j)$ obtained with an 8×8 grid:

$$C(i,j)=\frac{1}{M}\sum_{m=1}^{M}\left[\frac{1}{N}\sum_{n=1}^{N}A(m,n)\cdot conj(Ph(m+i,n+j))\right], \qquad (1)$$

where M=8, N=8, $A(m, n)$ is the EIOC amplitude image intensity of the $(m, n)_{th}$ pixel, and $Ph(m+i, n+j)$ is the EIOC phase image intensity of the $(m+i, n+j)_{th}$ pixel. The difference in their information content is emphasized by maximum cross-correlation value (~30%, as seen). Assuming a distribution of backscattering coefficients

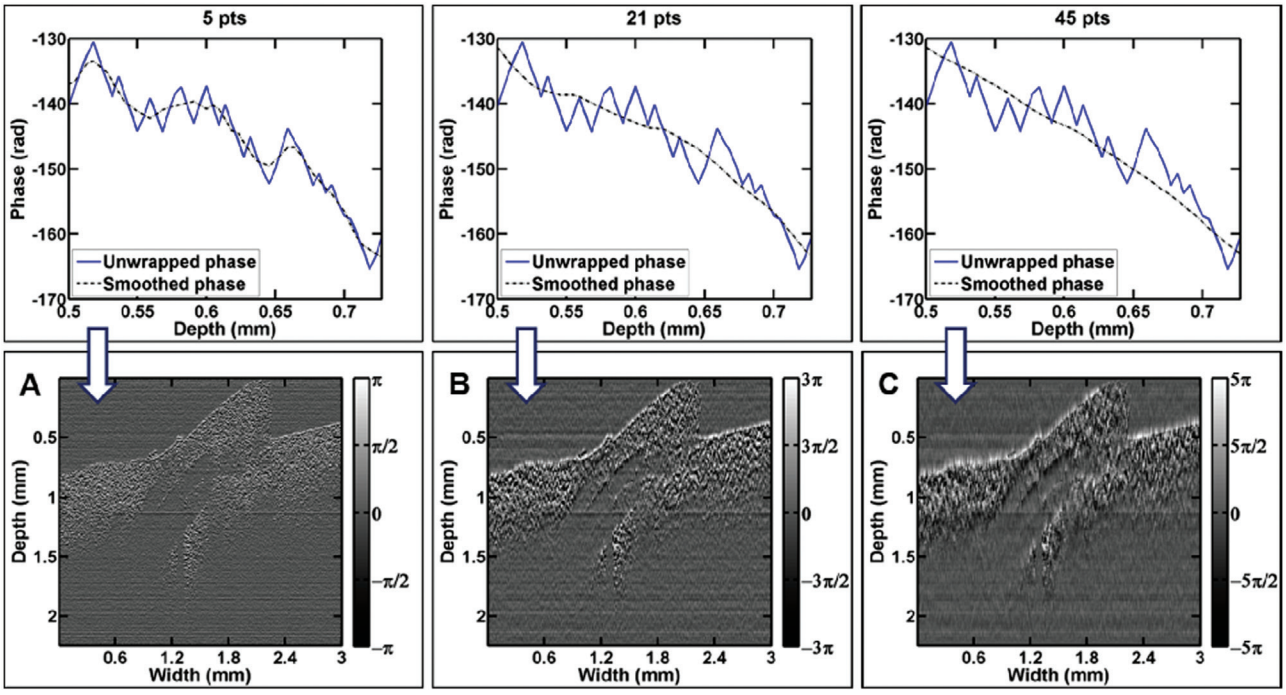

Figure 8 The different range for smoothing the phase curves in angular de-trending procedure and corresponding 2-D phase images: (A) 5 nearest points, (B) 21 nearest points, and (C) 45 nearest points. Phase images were obtained after averaging 110 angular de-trended phase frames before AC application. Gray bars on the right of each image indicate the resulting difference between unwrapped and smoothed curves in radians.

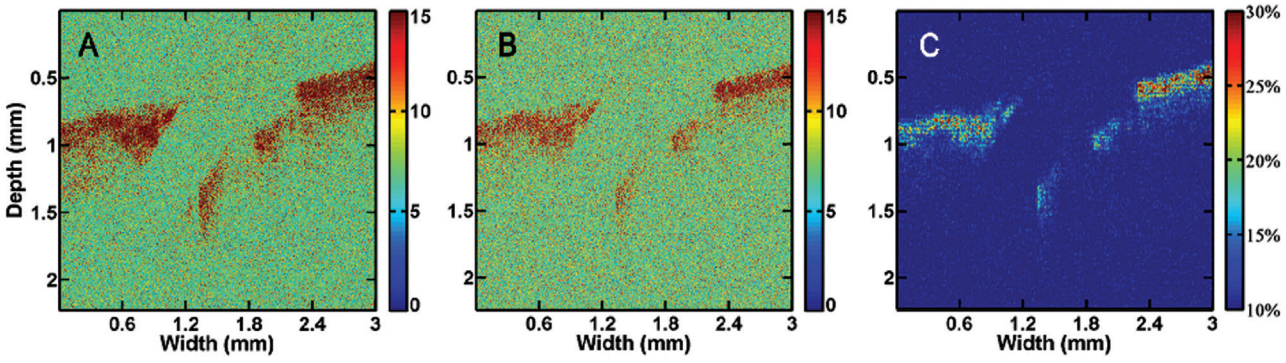

Figure 9 (A) Electrically induced optical changes (EIOC) amplitude image, (B) EIOC phase image, and (C) their cross-correlation image.

f(z) as a function of depth *z*, the measured spectrum *I(ω)* (*ω* is positive), can be approximated as the positive frequency components of the *F(ω)*, the Fourier transform of *f(z)* [28]. During our phase images derivation, an inverse Fourier transform to *I(ω)* to obtain *g(z)* is applied (note that in conventional OCT imaging, only the amplitude of *g(z)* is displayed). Since *I(ω)* contains positive frequency components of *F(ω)*, *g(z)* is essentially the Hilbert transform of *f(z)* [29]. Now it is known that for a modulated signal, the amplitude of its Hilbert transform gives the envelope of the signal, whereas Hilbert phase gives the information on the oscillation under the envelope. Therefore the phase of the OCT signals provides different/additional information on tissue properties, and phase images differ from amplitude images in our EIOC investigations.

The presented OCT phase measurements approach can be potentially used for identification and characterization of morphology and function of normal and pathologic tissues, specifically cancerous ones. Today there exists a variety of advanced imaging modalities for this purpose, including OCT, but standard structural OCT imaging cannot detect early pathological changes in tissues [30].

One of the potential methods for early detection of pathology is through changes in electro-kinetic properties of tissue on the cellular level [31]. It was experimentally shown that malignant transformation of cells is correlated to the changes in the fixed charge density (FCD) on cell membranes. It is also known that within the tumor, FCD is significantly larger than on cell membranes within normal tissue at different pH levels [32]. Ultrasound has also shown a similar correlation of FCD in the extracellular matrix with physiological and pathological changes in tissue [33]. Dolowy [34] has demonstrated that cell membrane charge increases during tumorogenesis and decreases during necrosis.

These previous studies and preliminary EIOC imaging results demonstrate a promising potential for monitoring the FCD changes within tissues with amplitude and phase OCT analysis through their electro-kinetic responses. Electro-kinetic phenomenon like electro-osmotic flow, may be used for measuring zeta potential and consequently, defining electro-kinetic properties of tissue [2]. Electro-osmotic flow is the liquid flow under the action of the external field E. In Smoluchowski's theory [35], the electro-osmotic velocity is given by

$$v_{eo} = \frac{\varepsilon_{rs}\varepsilon_0\zeta}{\rho}E, \quad (2)$$

where ζ is the zeta potential, ε_{rs} is the relative permittivity of tissue, ε_0 is the electric permittivity of vacuum, and ρ is the dynamic viscosity of the liquid. The velocity of this flow hypothetically may be measured by analyzing the OCT signal changes with the proposed algorithm.

There have been several published attempts to measure slow flows and quantify small velocities, both in OCT and in fluorescence microscopy fields [36–39]. Although promising results have been reported, it still remains a challenging task for OCT. In well-controlled fluorescence microscopy experiments, the developed algorithms are quite interesting but not directly applicable to OCT mainly because: 1) fluorescence confocal micrographs exhibit lower levels of image speckle compared to OCT images; 2) OCT images are obtained over much greater depth but with somewhat lower axial and lateral resolutions (and thus do not resolve individual scatterers); and 3) contrast-agent-free OCT reflectance imaging has different image contrast characteristics compared to exogenously labelled fluorescence micrographs.

Figure 10 demonstrates: a) the time course of an angular de-trended OCT signal phase at 1 mm depth below the tissue surface before, during (inside the solid square), and after the AC application (step 5 of the algorithm in Figure 3); b) the same but de-trended signal (step 6 of the algorithm in Figure 3); and c) the Fourier transforms

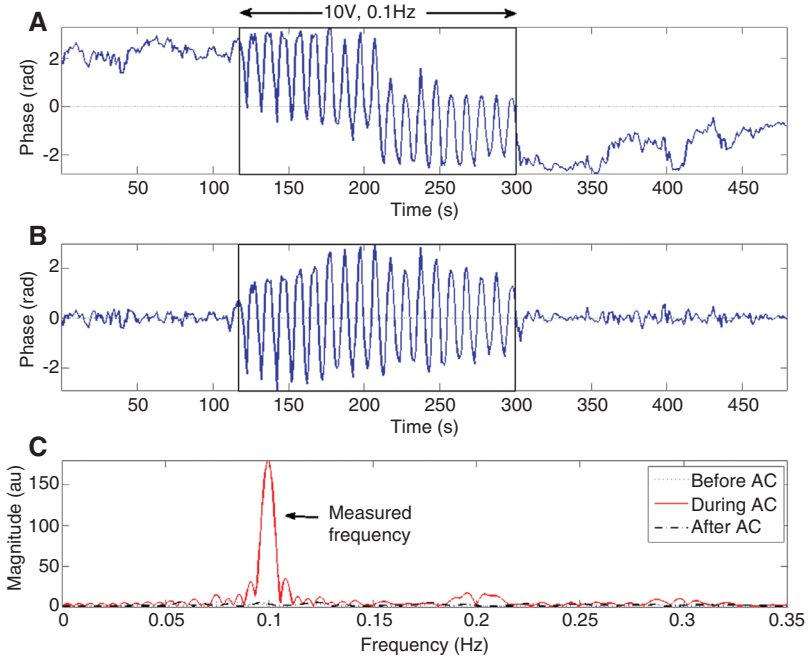

Figure 10 (A) The time course of an angular de-trended OCT signal phase at 1 mm depth below the tissue surface before, during (inside the solid square), and after the AC application (step 5 of the algorithm in Figure 3). (B) The same but de-trended signal (step 6 of the algorithm in Figure 3), and (C) Fourier transforms of de-trended signal portions before, during and after AC application (step 7 of the algorithm in Figure 3). Peak in the spectra marked "measured frequency" corresponds to the same frequency of the applied electric field (0.1 Hz).

of de-trended signal portions before, during and after AC application (step 7 of the algorithm in Figure 3). Conceptually, the electro-osmotic velocity may be estimated from the de-trended portion of the signal during AC application (Figure 10B) by calculating the slope m of the phase curve:

$$m=\frac{\varnothing_2-\varnothing_1}{t_2-t_1}, \quad (3)$$

where $\varnothing_1$ and $\varnothing_2$ are the initial and final phases, and t_1 and t_2 are the initial and final times of each cycle (as can be seen from Figure 10B, there are 18 cycles of signal phase change during AC application). If the phase curve is increasing (going up from left to right), its slope is positive. If the phase curve is going down (direction of external field changes), its slope is negative. The positive and negative slopes for each cycle may be related to the positive and negative electro-osmotic velocities, depending on the direction of the electric field applied to biological tissue. This conjecture requires further validation/testing before developing a metric for small velocities quantification.

5 Conclusion

The effects of a low-frequency electric field on 2D-OCT phase images of porcine heart samples were investigated in this study. The periodic changes in phase extracted from interference fringes during AC electric field application reflected the periodic change of the field at the same frequency.

The OCT signal phase processing method was developed, demonstrating the capability to image the electro-kinetic response of biological tissues to the external electric field. The multi-step procedure of removing the background noise from the EIOC images was introduced. The ability of the method to image the different levels of electro-kinetic responses of tissues was demonstrated using an electrically non-responding material (dielectric optical fiber) inserted into the tissue sample. EIOC images obtained after OCT amplitude and phase processing were found to be somewhat different from each other, each reporting on different aspects of the OCT interference signal. The availability of additional tissue characterization information via OCT phase analysis of the EKP effect was thus demonstrated.

The proposed technique may potentially prove useful for identification and characterization of morphology and function of cancerous tissues.

Acknowledgments: This research was supported by the Discovery Grants Program of the Natural Sciences and Engineering Research Council of Canada (Y. Xu and V. Toronov), the Canada Foundation for Innovation (V. Yang), and the Mathematics of Information Technology and Complex Systems (B. Vuong and C. Sun).

References

[1] Delgado AV, González-Caballero F, Hunter RJ, Koopal LK, Lyklema J; International Union of Pure and Applied Chemistry, Physical and Biophysical Chemistry Division IUPAC Technical Report. Measurement and interpretation of electrokinetic phenomena. J Colloid Interface Sci 2007;309(2):194–224.

[2] Lyklema J, editor. Fundamentals of interface and colloid science. Volume 5: Soft colloids. Amsterdam, San Diego, Oxford and London: Elsevier Academic Press; 2005.

[3] Gu WY, Lai WM, Mow VC. Transport of multi-electrolytes in charged hydrated biological soft tissues. Transport Porous Med 1999;34:143–57.

[4] Katnik C, Waugh R. Electric fields induce reversible changes in the surface to volume ratio of micropipette-aspirated erythrocytes. Biophys J 1990;57(4):865–75.

[5] Méthot S, Moulin V, Rancourt D, Bourdages M, Goulet D, Plante M, Auger FA, Germain L. Morphological changes of human skin cells exposed to a DC electric field in vitro using a new exposure system. Can J Chem Eng 2001; 79(4):668–77.

[6] Erickson CA, Nuccitelli R. Embryonic fibroblast motility and orientation can be influenced by physiological electric fields. J Cell Biol 1984;98(1):296–307.

[7] Doganay O, Xu Y. The effect of electric current in biological tissues on ultrasound echoes. Proceedings of the IEEE International Ultrasonics Symposium, Rome, Italy, 20–23 September 2009. doi: 10.1109/ULTSYM.2009.5441825.

[8] Doganay O, Xu Y. Electric-field induced strain in biological tissues. J Acoust Soc Am 2010;128(5):EL261–7.

[9] Doganay O, Xu Y. Reversibility of electric-field-induced mechanical changes in soft tissues. IEEE Trans Ultrason Ferroelectr Freq Control 2012;59(3):552–6.

[10] Youn JI, Akkin T, Milner TE. Electrokinetic measurement of cartilage using differential phase optical coherence tomography. Physiol Meas 2004;25(1):85–95.

[11] Wawrzyn K, Vuong B, Harduar MK, Yang VXD, Demidov V, Toronov V, Xu Y. Monitoring electric current in biological tissues by optical coherence tomography. Conference Paper. Biomedical Optics, Miami, FL, United States, April 28, 2012 – May 2, 2012. doi: 10.1364/BIOMED.2012.BW2A.4.

[12] Swatland HJ. Basic science for carcass grading. http://www3.sympatico.ca/howard.swatland/Brazil.htm [Accessed on July 21, 2014].

[13] Wawrzyn K, Demidov V, Vuong B, Harduar MK, Sun C, Yang VX, Doganay O, Toronov V, Xu Y. Imaging the electro-kinetic response of biological tissues with optical coherence tomography. Opt Lett 2013;38(14):2572–4.

[14] Peña AF, Devine J, Doronin A, Meglinski I. Imaging of the interaction of low-frequency electric fields with biological tissues by optical coherence tomography. Opt Lett 2013;38(14):2629–31.
[15] Fujimoto JG, Pitris C, Boppart SA, Brezinski ME. Optical coherence tomography: an emerging technology for biomedical imaging and optical biopsy. Neoplasia 2000; 2(1–2):9–25.
[16] Chinn SR, Swanson EA, Fujimoto JG. OCT using a frequency-tunable optical source. Opt Lett 1997;22(5):340–2.
[17] Gabriel C, Gabriel S, Corthout E. The dielectric properties of biological tissues: I. Literature survey. Phys Med Biol 1996;41(11):2231–49.
[18] Creath K. Phase-measurement interferometry techniques. In: Wolf E, editor. Progress in optics XXVI. Amsterdam: Elsevier Science Publishers B. V.; 1988, pp. 349–93.
[19] Takeda M, Ina H, Kobayashi S. Fourier-transform methods of fringe-pattern analysis for computer based topography and interferometry. JOSA 1982;72(1):156–60.
[20] Servin M, Marroquin JL, Cuevas FJ. Demodulation of a single interferogram by use of a two-dimensional regularized phase-tracking technique. Appl Opt 1997;36(19):4540–8.
[21] Gorthi SS, Rastogi P. Numerical analysis of fringe patterns recorded in holographic interferometry using high-order ambiguity function. J Mod Optic 2009;56(8):949–54.
[22] Kemao Q. Windowed Fourier transform for fringe pattern analysis. Appl Opt 2004;43(13):2695–702.
[23] Zhong J, Weng J. Dilating Gabor transform for the fringe analysis of 3-D shape measurement. Opt Eng 2004;43(4):895–9.
[24] Watkins LR, Tan SM, Barnes TH. Determination of interferometer phase distributions by use of wavelets. Opt Lett 1999;24(13):905–7.
[25] Rajshekhar G, Gorthi SS, Rastogi P. Adaptive window Wigner-Ville-distribution-based method to estimate phase derivative from optical fringes. Opt Lett 2009;34(20):3151–3.
[26] Reuss FF. Mémoires de la Société Impériale des Naturalistes de Moscou. Moscow 1809;2:327–44.
[27] Schmitt JM, Xiang SH, Yung KM. Speckle in optical coherence tomography. J Biomed Opt 1999;4(1):95–105.
[28] Tomlins PH, Wang RK. Theory, developments and applications of optical coherence tomography. J Phys D: Appl Phys 2005;38:2519–35.
[29] Titchmarsh EC. Introduction to the theory of Fourier integrals. Oxford: Clarendon Press; 1937.
[30] Fercher AF, Drexler W, Hitzenberger CK, Lasser T. Optical coherence tomography-principles and applications. Rep Prog Phys 2003;66(2):239–303.
[31] Szachowicz-Petelska B, Dobrzyńska I, Figaszewski Z, Sulkowski S. Changes in physico-chemical properties of human large intestine tumour cells membrane. Mol Cell Biochem 2002;238(1–2):41–7.
[32] Szachowicz-Petelska B, Dobrzynska I, Sulkowski S, Figaszewski Z. Characterization of the cell membrane during cancer transformation. J Environ Biol 2010;31(5):845–50.
[33] Insana MF, Pellot-Barakat C, Sridhar M, Lindfors KK. Viscoelastic imaging of breast tumor microenvironment with ultrasound. J Mammary Gland Biol Neoplasia 2004;9(4):393–404.
[34] Dolowy K. Biochemistry of cell surface. Progr Surf Sci 1984;15:245–368.
[35] Smoluchowski M. Elektrische Endosmose und Strömungsströme. In: Graetz L, editor. Handbuch der Elektrizität und des Magnetismus. Band 2. Leipzig: Johann Ambrosius Barth Verlag; 1921, p. 366–428.
[36] Shen ZY, Wang M, Ji YH, He YH, Dai XS, Li P, Ma H. Transverse flow-velocity quantification using optical coherence tomography with correlation. Laser Phys Lett 2011;8(4):318–23.
[37] Ruan Q, Cheng MA, Levi M, Gratton E, Mantulin WW. Spatial-temporal studies of membrane dynamics: scanning fluorescence correlation spectroscopy (SFCS). Biophys J 2004;87(2):1260–7.
[38] Carroll NJ, Jensen KH, Parsa S, Holbrook NM, Weitz DA. Measurement of flow velocity and inference of liquid viscosity in a microfluidic channel by fluorescence photobleaching. Langmuir 2014;30(16):4868–74.
[39] Hebert B, Costantino S, Wiseman PW. Spatiotemporal image correlation spectroscopy (STICS) theory, verification, and application to protein velocity mapping in living CHO cells. Biophys J 2005;88(5):3601–14.